Experiments and simulations of 4.5-keV Ar^{7+}-ion guiding through a conical glass macrocapillary

Nikolaus Stolterfoht,[1] Elisabeth Gruber,[2] Peter Allinger,[2] Stefan Wampl,[2] Yuyu Wang,[2,3]
Marius J. Simon,[4] and Friedrich Aumayr[2]

[1]*Helmholtz-Zentrum Berlin für Materialien und Energie, 14109 Berlin, Germany*
[2]*Institute of Applied Physics, Vienna University of Technology, 1040 Vienna, Austria*
[3]*Institute of Modern Physics, Chinese Academy of Sciences, Lanzhou, 730000 Gansu, China*
[4]*Labor für Ionenstrahlphysik, ETH Zürich, 8093 Zürich, Switzerland*

(Received 15 January 2015; published 16 March 2015)

Experimental and theoretical studies are performed to investigate guiding of 4.5-keV Ar^{7+} ions through a conical macrocapillary. The tilt angle of the capillary axis relative to the incident beam is varied within 0°–2°. The experiments are performed using a glass capillary whose bulk conductivity could be varied by changing its temperature from 24 °C–110 °C. At lower temperatures a minimum in the transmitted ion intensity is observed in the forward direction. After strongly increasing the electrical conductivity of the capillary by increasing its temperature to 110 °C, the transmission profile becomes geometrical without a forward minimum. The experimental data are compared with theoretical results, which are based on simulations previously developed for nanocapillaries and a straight macrocapillary. Both the surface and bulk conductivities are implemented in the calculations, providing clear evidence that the bulk conductivity is dominant. The major experimental features are reproduced by the simulations, providing evidence for the mechanisms producing the forward minimum.

DOI: 10.1103/PhysRevA.91.032705 PACS number(s): 34.50.Fa, 32.80.Fb

I. INTRODUCTION

After the first observation that keV ions are guided through insulating nanocapillaries [1], the topic has received considerable attention during the past decade [2]. Ions deposited at the capillary wall produce a repulsive electric field that is capable of deflecting the following ions at relatively large distance. Thus, the ions are guided along the capillary axis, maintaining their incident charge state. Ion guiding is based on a self-organizing process, which governs the charge deposition inside the capillaries. The incident ions produce a charge patch in the entrance region, which in turn increases until the ion deflection starts and the charge deposition decreases. Finally, at equilibrium, the charge deposition and the discharge via surface and bulk conduction is balanced.

The initial exploration of the ion-guiding phenomenon in insulating materials was performed using multiple capillaries [1,3–10]. These studies confirmed the capillary guiding for various materials and revealed the dominant properties of the guiding mechanisms. Moreover, guiding of charged particles was successfully performed with single straight capillaries [11–14], single tapered capillaries [15–17], and between parallel glass plates [18]. The work with tapered capillaries was motivated by the aim to produce a beam whose direction may be controlled in microscopic dimensions. Such beams are important for various applications, which include nanoscale modifications of surfaces [19], shaping of ions beams [20], focusing of exotic charged particle beams [21], and irradiation of single living cells [22].

Theoretical studies provided detailed information about capillary guiding. In a series of simulations [23–26], a diffusion model was used wherein the deposited charges perform a random walk along the surface and inside the bulk of the capillary. A different concept was adopted in recent simulations [27,28] involving a nonlinear charge transport at the capillary surface based on the formalism by Frenkel [29]. The simulations of nanocapillaries were extended to study guiding through a straight macrocapillary [30,31], for which the bulk conductivity was found to be dominant.

In general, the fraction $f(\psi)$ of transmitted ions at equilibrium decreases exponentially with the square of the tilt angle ψ similar to a Gauss function. The guiding power can be accounted for by the characteristic guiding angle ψ_c, for which the normalized transmission fraction drops as $f(\psi_c)/f(0) = 1/e$. In specific cases of macrocapillaries, an intensity minimum was observed at zero tilt angle ($\psi = 0$) by Nakayama *et al.* [13] and Kreller *et al.* [17]. In the latter work, the transmission curves could be fitted by a difference of two Gauss functions. The intensity minimum was qualitatively explained by the repulsive Coulomb force of a uniformly charged region within the capillary, which is supposed to block the ion transmission.

Progress in the field of capillary guiding was recently achieved in experiments by Gruber *et al.* [14] using a straight capillary from borosilicate glass (Duran) [32]. The capillary conductivity was controlled by heating or freezing the capillary material. Most models describing the charge transport in an insulator (such as that by Frenkel [29]) predict a very strong temperature dependence of both the surface and the bulk conductivity. This dependence could be used to vary the conductivities by as much as four orders of magnitude [14].

In this work, experiments and simulations of the ion transmission through a macroscopic conically shaped tapered capillary were performed. Preliminary results have been presented in Ref. [33]. By changing the capillary conductivity with its temperature, the present experiments are similar to those for a straight glass capillary [14]. Around room temperature the ion transmission shows a minimum at zero tilt angle, which is interpreted by simulations based on a code previously developed [30,31]. At lower temperatures the guiding effect causes a focusing of the ions, which increases the current density by more than a factor of 3.

II. EXPERIMENTAL METHOD

The measurements have been performed in a UHV chamber situated at the Institute of Applied Physics at TU Wien. The chamber was operated with a base pressure below 5×10^{-9} mbar. To study the temperature dependence, a proper heatable capillary holder was constructed. The capillary was placed in a specially designed thermoshielded copper cylinder surrounded by stainless steel coaxial heaters. Shown in Fig. 1(a) is the experimental set up and in Fig. 1(b) is a detailed view of the capillary heater.

The temperature of the copper parts is monitored by a K-type thermocouple and the heating power regulated by the proportional-integral-derivative controlled heater. The resulting magnetic field of the solenoid configuration of these heating wires has been estimated and its effect on the ion-beam trajectories simulated with the software SIMION 8.0 [34]. With heating currents of a few amperes, the influence on the ion trajectories was found to be negligible.

In the measurements a single tapered macroscopic capillary, made of borosilicate glass, was used as shown in Fig. 1(c). The capillary was fabricated at ETH Zürich by means of a microforge. The entrance diameter of the conical shaped capillary is 860 μm, while the exit diameter is 82 μm. The wall thickness decreases linearly from 320 μm (entrance) to 24 μm (exit). A 5-mm-long straight section of the capillary is followed by a 50-mm-long conical part. In order to achieve a defined field distribution, the outer wall of the capillary is covered with graphite. The experimental setup allows a controlled and uniform temperature variation of the glass capillary between 24 °C and 110 °C (297 K $\leqslant$ T $\leqslant$ 383 K) and thus a variation of the conductivity by almost three orders of magnitude [14,35].

The 4.5-keV Ar^{7+} ions are provided by the ECR ion source in Vienna [36]. The extracted ion beam is focused, mass-to-charge separated by a sector magnet, and afterward guided into the experimental chamber. The ion optical system of the experimental chamber consists of a collimator and a lens system with several sets of deflection plates and apertures as indicated in Fig. 2. The collimator restricts the angular divergence of the ion beam to less than ±0.25° half width at half maximum (HWHM). However, the exact value of the beam divergence at the entrance of the capillary is difficult to determine, because it depends on further focusing elements of the ion optical system.

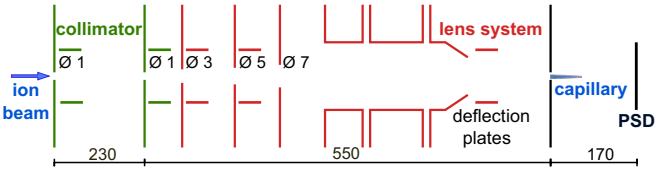

FIG. 2. (Color online) Schematic view of the ion optical system (not to scale); the ion beam is collimated to an angular divergence of less than ±0.25°, transported, and focused by the lens system with several sets of deflection plates and apertures onto the capillary's entrance. The transmitted ions are detected by the PSD. All dimensions are given in mm.

Directly in front of the capillary the ion beam is collimated by a metallic entrance aperture to avoid the charging of the glass front of the capillary. This entrance aperture has a diameter of about 800 μm. The beam-spot diameter at this position is about 2.5 mm. For beam diagnostic and monitoring purposes, two reference apertures of different diameters (800 and 100 μm diameter) can be inserted into the beam instead of the capillary. A position-sensitive microchannel-plate detector (PSD) of 50 mm diameter with a wedge-and-strip anode measures the transmitted ions.

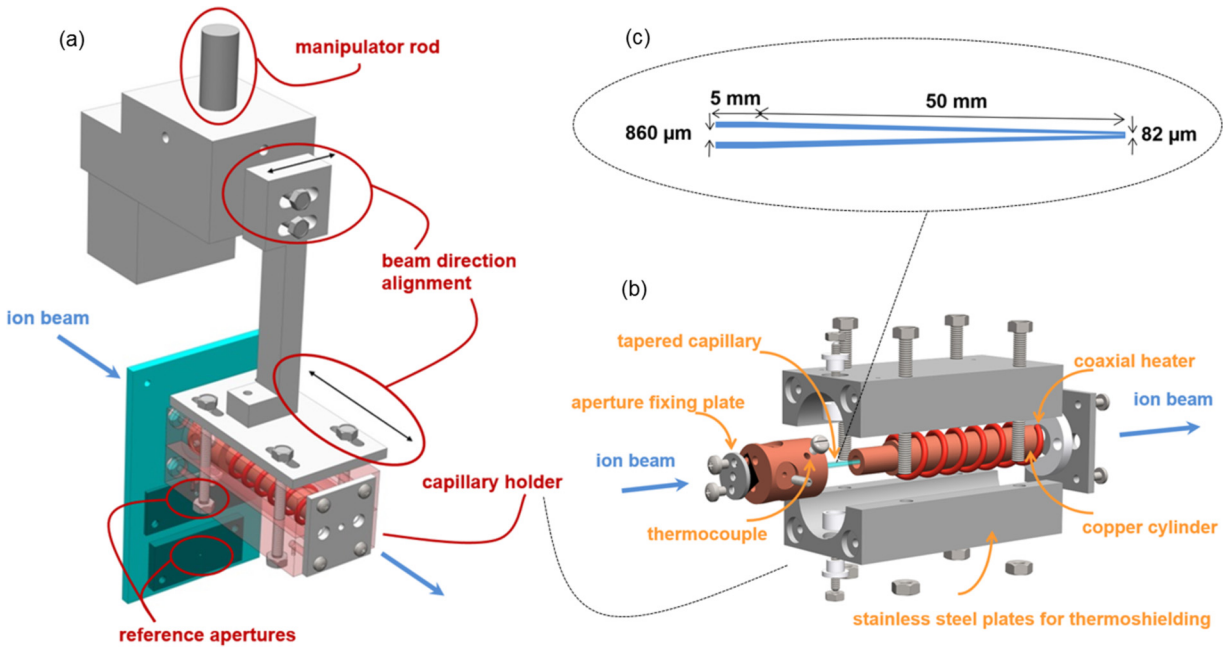

FIG. 1. (Color online) View of the heatable capillary holder. (a) Experimental setup. (b) The capillary is placed in a copper cylinder surrounded by stainless steel coaxial heaters. (c) Geometric data of the conically shaped glass capillary.

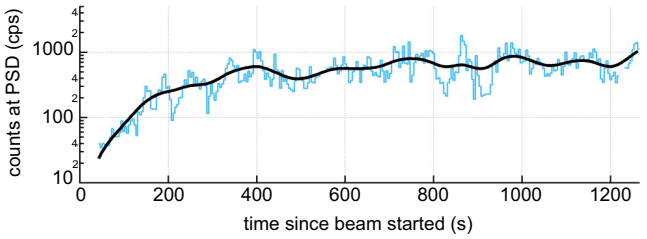

FIG. 3. (Color online) Temporal evolution of the ion count rate at the PSD obtained with a constant incident beam. The capillary tilt angle is 2°. The measurements are performed at room temperature.

Before starting the proper measurements, the alignment of the capillary axis along the incident ion-beam direction is performed. Since the capillary can only be tilted in one plane, the straight direction can be found by heating the capillary or, in other words, by increasing the electrical conductivity. At sufficiently high temperatures (typically 100 °C) the guiding effect vanishes [14] and the transmission curve is simply given by the geometric transmission through the capillary. At this point the straight incident direction can be determined by optimizing the transmitted ion intensity while steering the incoming beam with several pairs of electrostatic deflection plates.

Afterward the capillary is cooled down and transmission curves are recorded at some fixed temperatures. In steps of usually less than 1° the capillary is tilted in one direction and the data are stored until the transmission becomes negligible. Subsequently, the capillary is stepwise tilted back in the opposite direction until the transmission vanishes again. For each tilt angle, transmission rates are recorded after equilibrium conditions (i.e., a constant count rate) are reached.

In Fig. 3(a) typical example for the temporal evolution of the count rate is shown. The blue line represents the measured count rate over the elapsed time and is smoothed by the black line. As soon as the beam is turned on, the count rate of the transmitted ions is recorded. The total ion count rate onto the detector is summed up and is dead-time corrected. During one measurement period the incident ion flux is kept constant and controlled by monitoring the beam intensity on the collimation diaphragms. After a charging time of approximately 400 s, a saturation value is reached (Fig. 3). The ion current incident into the capillary is estimated to be ∼100 fA. Hence, with this incident flux, equilibrium transmission is achieved after a few minutes.

III. EXPERIMENTAL RESULTS

Figure 4 depicts tilt angle dependences of the transmitted ion intensity for which the temperature of the capillary was varied from 24 °C to 110 °C. Measurements at room temperature indeed show a minimum of the transmission in the forward direction close to $\psi = 0°$. Such a forward intensity drop has been observed previously [10,13], wherein it has been explained qualitatively by repulsive Coulomb forces of a uniformly charged ring-shaped region in the tapered part of the capillary that supposedly is blocking the transmission. We interpret the minimum by a different mechanism presented further below in Sec. V.

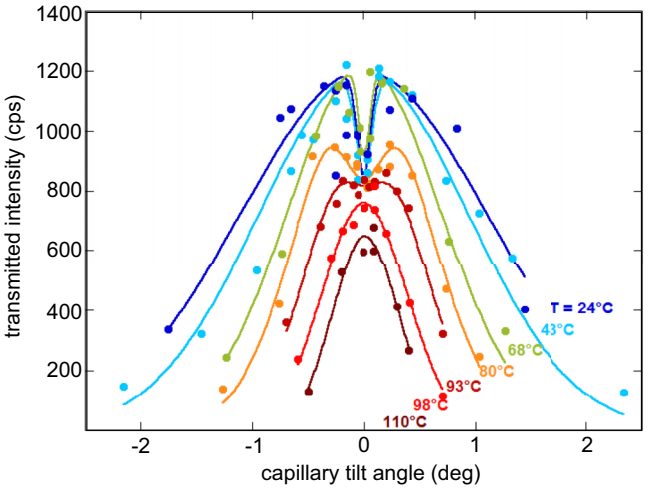

FIG. 4. (Color online) Transmission curves for 4.5-keV Ar^{7+} ions guided through the tapered glass capillary for different capillary temperatures. The flux of the incident ions was kept constant. The data points are fitted by the Gaussian ansatz (lines) given in Eq. (1).

The measured transmission curves can be fitted by the Gaussian ansatz

$$f(x) = a \exp\left(-\frac{x^2}{2\psi_1^2}\right) - \left| b \exp\left(-\frac{x^2}{2\psi_2^2}\right)\right|, \qquad (1)$$

with $b < a$ and $a, b > 0$. The parameter ψ_1 is the guiding angle of the Gaussian ansatz. Values of the parameters a, b, ψ_1, and ψ_2 have been given previously [33]. The second part of the fit function represents the suppression of the transmission at small tilt angles. The parameters b and ψ_2 characterize, respectively, the magnitude and the width of the transmission minimum in the forward direction.

The systematic series of measurements at different capillary temperatures show the well-known effect that an increase of the electrical conductivity leads to a decrease of the guiding power [14] because the charge patches necessary for guiding are no longer formed. Furthermore, the increase of the capillary temperature up to about 100 °C disperses the minimum in the transmission curve so that the transmission has its maximum in the forward direction (Fig. 4). However, this maximum in (geometric) transmission is still smaller by ∼25% than the reduced transmitted intensity in the forward direction at room temperature. This leads to the conclusion that at room temperature the focusing effect in the forward direction due to the guiding dominates and is only partially weakened by blocking. By tilting the capillary by only 0.1°–0.2° the symmetry of the charge deposition is broken and the transmission is enhanced by almost a factor of 2 as compared to the optimum geometric transmission.

IV. ESSENTIALS OF THE SIMULATIONS

The simulations were carried out using methods previously developed for nanocapillaries [27,28] and a straight macrocapillary [30]. Ions trajectories were evaluated in three dimensions for the conical capillary shown in Fig. 1(c) by solving Newton's equation of motion. The ions were inserted under the tilt angle ψ starting with random x and y values

within the circular entrance of the capillary. A divergence of the incident angle was imposed on the incident beam. The electric potential within the capillary was evaluated by adding the Coulomb potentials of the individual charges deposited on the capillary surface. The potential was differentiated analytically with respect to the x, y, and z coordinates yielding the electric field components E_x, E_y, and E_z, respectively.

As mentioned, the calculations for a macrocapillary are very time consuming. To drastically reduce the computer time, several thousand ion charges were assumed to be deposited per ion hitting the capillary wall as previously done for a straight macrocapillary [30]. To ensure that this approximation is feasible, the number of deposited charges was varied using $1000q$,$2000q$, and $5000q$, where q is the ion charge. The ion trajectories were not much affected by the cluster size, as the mean distance between the clusters is significantly smaller than the capillary diameter. The charge variation primarily influenced the statistics of the electric potential, whereas the essential properties of the ion guiding remained unchanged. Thus, the calculations were generally performed with $5000q$.

As described in conjunction with Fig. 1(c), the outer wall of the capillary is covered with graphite. The grounded metal layer at the glass wall affects the field within the capillary. The conducting layer is taken into account by adding images of the deposited charges using the layer as a mirror. The major effect of the negative image charges is the potential drop to zero at the metal layer. Moreover, to achieve stable guiding conditions, the charges deposited within the capillary are depleted by decay mechanisms. Both bulk and surface conductivities are implemented into the calculations as described in more detail previously [27].

The present simulations clearly show that the main depletion effect is due to the charge migration into the capillary bulk. This charge depletion can be treated like the discharge of a capacitor by the current flowing through the dielectric material (Duran) separating the deposited charges from the outer metal layer. The decay rate Γ_b for the deposited charges due to the bulk conductivity σ_b is obtained as [26,30]

$$\Gamma_b = c_{sr}\frac{\sigma_b}{\varepsilon_0}, \tag{2}$$

where ε_0 is dielectric constant and $c_{sr} = 2/(\varepsilon_r + 1)$ is a screening factor for the deposited charges due to the relative dielectric constant ε_r of Duran.

It is pointed out that Γ_b is independent of the density of the deposited charge, so the size of the charge clusters does not influence their decay. Moreover, Γ_b is independent of the capacitor geometry, so it does not depend on the wall thickness, which changes for the conical capillary [Fig. 1(c)]. Hence, it follows that the same decay rate applies for all locations within the capillary, which significantly simplifies the calculations.

The simulations were performed at different temperatures given in the first column of Table I. Each temperature corresponds to a specific bulk conductivity determined experimentally [14] as shown in the second column. Then the decay rate Γ_b was derived by means of Eq. (2) and is given in the third column. As an example, at a room temperature of 24 °C, with the values of $\sigma_b = 8.6 \times 10^{-16}$ S/cm [14], $\varepsilon_r = 4.6$ for Duran [32], and $\varepsilon_0 = 8.8 \times 10^{-14}$ C/V cm, one obtains a decay rate of $\Gamma = 3.5$ mHz, which corresponds to a mean survival time of 280 s for the deposited charges. It is seen that the decay rate can be changed by several orders of magnitude by varying the capillary temperature.

TABLE I. Temperature and corresponding bulk conductivity measured in [14]. The decay rates were derived using Eq. (2)

Temperature (°C)	Conductivity (S/cm)	Decay rate (mHz)
24	8.6×10^{-16}	3.5
33	2.45×10^{-15}	10
45	7.4×10^{-15}	30
56	2.46×10^{-14}	100
80	2.46×10^{-13}	1000
110	3.5×10^{-12}	14000

As in previous simulations [27,28,30], the ion insertion and the charge transport were treated sequentially in small portions. After the arbitrary number of $n_0 = 20$ ions were inserted into the capillary, the deposited charges were attenuated during the time equal to the insertion time Δt of the n_0 ions. This time is given by

$$\Delta t = \frac{q_d\, n_0}{J_{in}}, \tag{3}$$

where q_d is the deposited charge per incident ion and J_{in} is the ion current. As noted the incident beam current was $J_{in} \approx 100$ fA, corresponding to $\Delta t = 1.1$ s with $n_0 = 20$, $q_d = 5000q$, and $q = 7$. Except for some test calculations, these parameters were kept constant throughout the present work.

It should be emphasized that in the simulations the bulk discharge is uniquely governed by the probability for depleting the deposited charges during the interval Δt, which is obtained as

$$p_b = 1 - \exp(-\Gamma_b \Delta t). \tag{4}$$

For room temperature with $\Gamma_b = 3.5$ mHz, it follows that $p_b \approx 0.004$, which is sufficiently small to avoid instabilities in the calculations. For higher temperatures with $\Gamma_b \gtrsim 1000$ mHz, p_b approaches unity, so practically no deposited charges remain in the capillary.

From Eq. (4) it readily follows that the total charge Q remaining at the capillary wall after the insertion of the charge Q_{in} is given by [1]

$$Q = Q_\infty\left[1 - \exp\left(-\frac{Q_{in}}{Q_\infty}\right)\right], \tag{5}$$

where $Q_\infty = J_{in}/\Gamma_b$ is the asymptotic charge obtained at equilibrium. This expression is valid for the case a capillary discharge by bulk conductivity governed by Ohm's law. Moreover, it is important to note that the results of the simulations depend on the ratio Γ_b/J_{in}. Hence it is redundant to perform calculations changing J_{in} as well as Γ_b. In this work, the discharge rate Γ_b was varied (Table I), whereas J_{in} was kept constant.

V. RESULTS OF THE SIMULATIONS

A. Trajectories and charge distributions

In the following, characteristic results of the simulations are presented. The calculations were performed using 4.5-keV Ar^{7+} ions incident on the conical capillary depicted in Fig. 1(c). Moreover, the tilt angle and the decay rate were varied in accordance with the experimental conditions. The divergence of the beam was assumed to be $\pm 0.25^\circ$ HWHM. Examples for other beam divergences will be given at the end of the data presentation.

In Fig. 5 ion trajectories and deposited charges are plotted along the capillary length. Note from the horizontal and vertical scales that the aspect ratio is significantly changed for graphical reasons. Results are given for different decay rates $\Gamma_b = 10$, 30, and 100 mHz of the deposited charges, which are associated with temperatures of 33 °C,45 °C, and 56 °C, respectively (see Table I). The capillary tilt angle was equal to 0°, i.e., the ions were inserted parallel to the capillary z axis. Each of the graphs on the left-hand side shows 20 ion trajectories. In the top and middle graphs, the trajectories appear to be focused just before leaving the capillary exit, whereas in the bottom graph the ions are emitted more parallel to the capillary axis.

The distributions of deposited charges are shown in the right-hand graphs of Fig. 5 wherein each dot symbolizes 35 000 positive elementary charges. The pictures were taken after charge insertion of about 20 pC, i.e., under equilibrium conditions for which the total accumulated charge does not change anymore. It can be seen that the charge density strongly decreases with increasing decay rate in accordance with Eq. (5). The charge accumulation will be discussed in more detail further below.

Figure 6 shows trajectories and charge distributions for the tilt angles $\psi = 0.2^\circ$,0.5°, and 1° and the decay rate of 10 mHz. This series of pictures should be considered together with the top panel in Fig. 5 associated with the tilt angle of 0°.

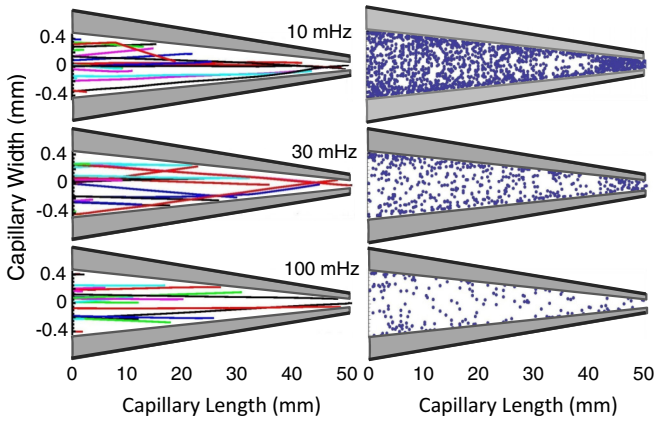

FIG. 5. (Color online) Trajectories and charge distribution of 4.5-keV Ar^{7+} ions traversing the conical capillary shown in Fig. 1(c). The data are obtained with discharge rates 10, 30, and 100 mHz given in the figure. The tilt angle is 0° and the divergence of the incident beam beam is $\pm 0.25^\circ$ (HWHM). Each panel on the left-hand side contains 20 trajectories. Each dot in the panels of the right-hand side corresponds to 35 000e.

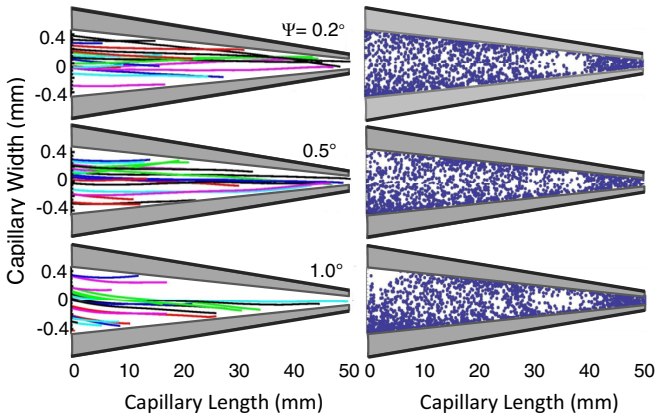

FIG. 6. (Color online) Trajectories and charge distributions of Ar^{7+} ions traversing the conical capillary. The data are obtained with tilt angles of 0.2°,0.5°, and 1° as indicated in the figure. The decay rate is 10 mHz. For more information see the caption of Fig. 5.

Again the graphs on the left-hand side show ion trajectories calculated with the charge distribution visualized on the right-hand side. As in Fig. 5, the charge insertion amounts to 20 pC for which equilibrium was achieved. For the nonzero tilt angles the trajectories are slightly deflected so that they can reach the capillary exit. This deflection is due to an enhancement of the charge deposition on the lower part of the capillary, which produces a field component in the y direction perpendicular to the capillary axis.

The characteristic feature of the present charge distributions is the relatively weak charge deposition along the z coordinate between 30 and 40 mm and the corresponding charge enhancement near the capillary exit. Evidently, the ions trajectories are guided within the capillary with a focus point at some distance before the capillary exit. Within the focus point the charge deposition is attenuated, whereas after the focus point the deposition is enhanced. This finding is most likely the key for the understanding of the characteristic ion transmission showing a minimum in the forward direction. We shall return to this scenario after looking at the potential created in the capillary.

B. Total charge and potential

To obtain more quantitative information about the transmitted ions, specific properties of the capillary were studied. In particular, the total charge accumulated within the capillary and the corresponding potential were extracted as side results of the simulations. The total charge can be compared with the expression in Eq. (5) providing a simple test for basic properties of the simulations.

In Fig. 7 the total charge Q integrated over the inner wall of the capillary is plotted as a function of the inserted charge Q_{in}. Because of $Q_{in} = J_{in}t$, the dependence on Q_{in} can also be regarded as a temporal evolution. The results were obtained with the discharge rates of 3.5, 30, and 100 mHz corresponding to the capillary temperature of 24 °C,45 °C, and 56 °C, respectively. In the simulations, data are derived for tilt angles of 0° and 1° represented by closed circles and squares,

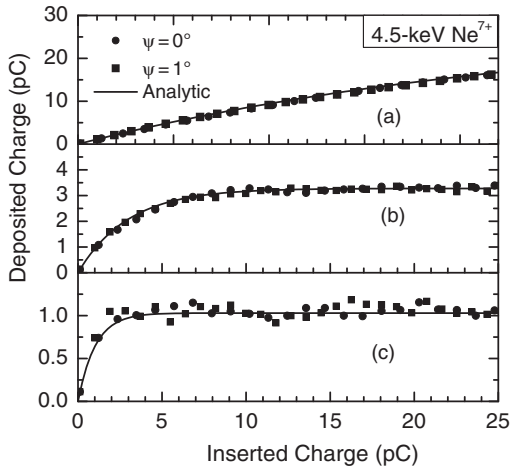

FIG. 7. Total charge Q accumulated in the capillary as a function of the inserted charge Q_{in}. Closed circles and squares represent simulations for the tilt angles of 0° and 1°, respectively. The results are compared with the analytical function given by Eq. (5) (solid line). The data are obtained for the discharge rates of (a) 3.5, (b) 30, and (c) 100 mHz as indicated in the figure.

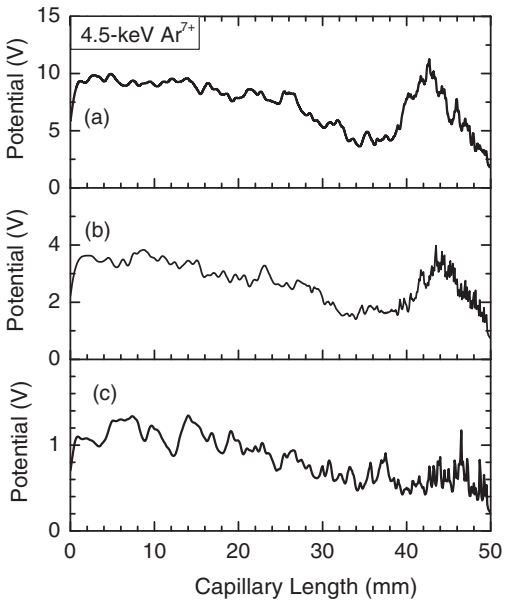

FIG. 8. Potential in the center of the capillary as a function of the z coordinate. Equilibrium conditions are attained and the tilt angle is 0°. Results are obtained for discharge rates Γ_b of (a) 3.5, (b) 10, and (c) 30 mHz.

respectively. As expected, the results for the two tilt angles are equal within the statistical uncertainties.

In Fig. 7 the results of the simulations are found to agree very well with the predictions of the analytic expression (5) given as solid lines. This confirms that the asymptotic charge and the charge constant, characteristic for the initial rise of Q, are given by the same parameter Q_∞, which is inversely proportional to Γ_b. It should be realized that the analytic expression (5) is free of an adjustable parameter. The present agreement provides evidence that the discharge of the capillary proceeds primarily via bulk conductivity with a linear field dependence. The dominance of the bulk conductivity could directly be proven by the simulations as it implies both surface and bulk conductivities.

In Fig. 8 examples for the electric potential in the capillary center are plotted along the capillary z axis. Discharge rates are the same as before. In Fig. 7 the equilibrium charge was found to be inversely proportional to Γ_b. The same dependence on Γ_b is found for the potential, indicating that both quantities are closely related. It is noted that the potential barely changes when traced along x and y axes within the capillary. Thus, the corresponding field components are small. An exception exists for tilted capillaries, whose y field component near the capillary entrance is sufficiently strong to deflect the incident ions to the exit.

The curves in Fig. 8 exhibit a minimum in the z axis range from 30 to 40 mm and a maximum around 45 mm. These structures are more pronounced for decreasing decay rate. They are consistent with the charge distributions plotted in Fig. 5. There, minima and maxima have been explained by focusing effects on the ions with a focal point within the minimum. It should be added that the potential maximum is much smaller than the potential that would be necessary to fully suppress the transmission of a keV ion.

C. Tilt angle dependence

In the following, the calculated fraction of transmitted ions is compared with the experimental results as a function of the tilt angle. This fraction was obtained as the number of transmitted ions normalized to the number of incident ions. Since the geometric opening of the capillary outlet amounts to 0.9% of the inlet opening [Fig. 1(c)], only about 1 out of 100 incident ions pass the exit of the capillary. Hence the present calculations require more effort to achieve adequate statistics than the work with straight capillaries [30].

In particular, due to limited statistics, it was not possible to determine angular distributions of the ions ejected from the capillary exit. Thus, only ion fractions integrated over the emission angle are shown. Also, the limited statistics does not allow definite conclusions about temporal evolution of the ion yields. It appears that, except for the data derived for tilt angles of 0.7° and 1°, equilibrium is reached immediately after insertion of less than 1 pC, which corresponds to a few minutes (with the incident current of 0.1 pA). This time dependence is consistent with the experimental observations.

In Fig. 9 the calculated ion fraction is plotted for different decay rates corresponding to temperatures ranging from 24 °C to 110 °C. For the highest temperature the bulk conductivity is so large that no charge remains on the inner surface of the capillary. Thus, the ion trajectories are straight lines and the ion fraction is equal to the ratio of the geometric capillary openings. At lower temperatures the ion fractions are as high as 2.2%, which provides evidence that the ions are guided and focused by the field of the accumulated charges.

The simulations are compared with experimental results that are normalized at the calculated maximum of the 30-mHz data. This latter normalization was also used for the experimental data measured at the highest temperature of

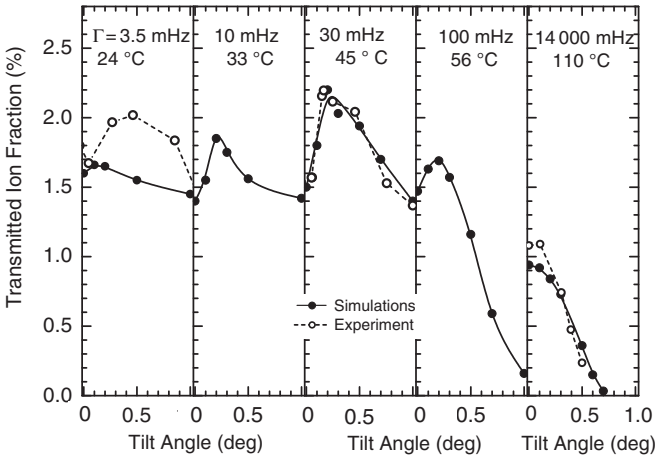

FIG. 9. Calculated ion fraction f in percent as a function of the tilt angle. The closed and open circles represent results from simulations and experiment, respectively. Data are obtained under equilibrium conditions for discharge rates of 3.5, 10, 30, 100, and 14 000 mHz. The corresponding temperatures are also shown. The beam divergence is equal to $\pm 0.25^\circ$ HWHM.

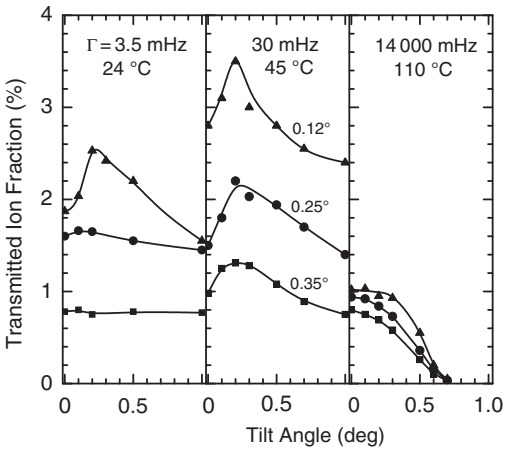

FIG. 10. Calculated ion fraction f as a function of the tilt angle. The closed triangles, circles, and squares represent results for divergences of $\pm 0.12^\circ$, $\pm 0.25^\circ$, and $\pm 0.35^\circ$, respectively. Data are given for discharge rates of 3.5, 30, and 14 000 mHz together with the corresponding temperatures.

110 °C. It is seen that the agreement between the results of the simulations and experiment is quite good, indicating that both sets of data follow geometric rules. However, it is noted that the simulations predicts a field-free capillary already for 80 °C (i.e., 1000 mHz), whereas the experimental curve indicates still guiding effects (Fig. 4).

The minimum in the transmission curve in the forward direction, which is the remarkable feature of the experimental curves, is reproduced by the simulations. For the temperature of 45 °C (discharge rate of 30 mHz) the agreement between experiment and theory is excellent. As expected, for 110 °C the minimum disappears for both experiment and simulations. However, for 24 °C (3.5 mHz) the minimum in the forward direction in the experimental curve is not reproduced by simulations. Rather, it predicts a nearly constant tilt angle dependence. This discrepancy may be attributed to the influence by the beam divergence.

In the experiments, exact values of the beam divergence are difficult to determine. The divergence depends on focusing elements and collimation slits defining the beam shape. From the experimental conditions the divergence was estimated to be $\pm 0.25^\circ$ HWHM for which most of the present results have been derived. To verify the influence of the beam divergence, additional calculations were performed for $\pm 0.12^\circ$ and $\pm 0.35^\circ$ HWHM. In Fig. 10 the results are shown for the decay rates of 3.5, 30, and 14 000 mHz.

The data show that the transmitted ion fraction significantly increases with decreasing divergence. For 45 °C (30 mHz) the transmission curve is enhanced to values as large as 3.5%. On the other hand, at 110 °C the results for the different divergences are nearly equal, being close to the expected geometrical value of 0.9%. At room temperature (3.5 mHz) the ion fractions differ in their tilt angle dependences. For divergences of $\pm 0.25^\circ$ and $\pm 0.35^\circ$ the data indicate no significant minimum at zero degree. However, the highest curve with a divergence of $\pm 0.12^\circ$ exhibits a minimum in the forward direction in accordance with the experimental data (Fig. 4).

VI. CONCLUSION

In this work, experiments and simulations for ion guiding through a conical macrocapillary are compared. In the experiments the capillary temperature was varied to control the conductivity of the capillary material. Thus, the rate for depleting the charges accumulated in the capillary could be changed dramatically. The simulations show that the charge accumulation is significant at 24 °C, whereas a temperature of 110° produces a high conductivity, which removes all charges from the capillary inner surface. In the latter case, the ions move on straight trajectories and their transmission follows geometric rules.

At lower temperatures the accumulated charges produce electric fields that are capable of guiding the ions to the capillary exit. The ion trajectories are focused so that the transmitted ion fraction is increased. The simulations show that the geometric ion transmission of 0.9% is enhanced to values from 2% to 3% depending on the beam divergence. The strong influence of the beam divergence is a remarkable result of the simulations, which demands further studies.

The experimental results exhibit a minimum in the transmission curves in the forward direction in accordance with the simulations. The calculated charge distributions show a maximum near the capillary exit and a minimum just before that. This observation provides evidence that the ions are focused at a point inside the capillary near its exit weakening the ion transmission. Evidently this overfocusing effect is stronger for the untilted capillary, so a minimum at forward angles occurs. For a tilted capillary a certain focal point still exists in front of the capillary exit (Fig. 6), however, the ion transmission appears to be less weakened near 0.2°.

The simulations show that the enhancement of the ion transmission is larger at 45 °C than at 24 °C. In the latter case (room temperature) the minimum in the transmission curve

disappears as the divergence of the ion beam increases. This is likely due to a stronger focusing of the ion trajectories as the charge compilation in the capillary is significant at room temperature. In this case more detailed work would be desirable to compare the simulations with experimental results.

Altogether, it is concluded that the minima in the forward direction, observed experimentally and theoretically, are due to overfocusing effects. It should be emphasized that this overfocusing involves deflection angles smaller than 1°. Thus, the scenario that the ions are fully blocked due to a large electrostatic field is inapplicable. The maximum potential created in the capillary is by far smaller than that required for a complete electrostatic blocking of keV ions.

ACKNOWLEDGMENT

The authors would like to thank Peter Hischenhuber for his help in constructing the heatable capillary holder. N.S. is indebted to Eric Giglio for helpful discussions concerning the simulations.

[1] N. Stolterfoht, J. H. Bremer, V. Hoffmann, R. Hellhammer, D. Fink, A. Petrov, and B. Sulik, Phys. Rev. Lett. **88**, 133201 (2002).
[2] C. Lemell, J. Burgdörfer, and F. Aumayr, Prog. Surf. Sci. **88**, 237 (2013).
[3] N. Stolterfoht, R. Hellhammer, Z. D. Pešić, V. Hoffmann, J. Bundesmann, A. Petrov, D. Fink, and B. Sulik, Vacuum **73**, 31 (2004).
[4] M. B. Sahana, P. Skog, G. Víkor, R. T. RajendraKumar, and R. Schuch, Phys. Rev. A **73**, 040901(R) (2006).
[5] S. Mátéfi-Tempfli, M. Mátéfi-Tempfli, L. Piraux, Z. Juhász, S. Biri, É. Fekete, I. Iván, F. Gáll, B. Sulik, G. Víkor *et al.*, Nanotechnology **17**, 3915 (2006).
[6] N. Stolterfoht, R. Hellhammer, J. Bundesmann, D. Fink, Y. Kanai, M. Hoshino, T. Kambara, T. Ikeda, and Y. Yamazaki, Phys. Rev. A **76**, 022712 (2007).
[7] P. Skog, I. L. Soroka, A. Johansson, and R. Schuch, Nucl. Instrum. Methods Phys. Res. Sect. B **258**, 145 (2007).
[8] Y. Kanai, M. Hoshino, T. Kambara, T. Ikeda, R. Hellhammer, N. Stolterfoht, and Y. Yamazaki, Nucl. Instrum. Methods Phys. Res. Sect. B **258**, 155 (2007).
[9] N. Stolterfoht, R. Hellhammer, Z. Juhász, B. Sulik, V. Bayer, C. Trautmann, E. Bodewits, A. J. de Nijs, H. M. Dang, and R. Hoekstra, Phys. Rev. A **79**, 042902 (2009).
[10] M. Kreller, G. Zschornak, and U. Kentsch, J. Phys.: Conf. Ser. **163**, 012090 (2009).
[11] R. Bereczky, G. Kowarik, F. Aumayr, and K. Tökési, Nucl. Instrum. Methods Phys. Res. Sect. B **267**, 317 (2009).
[12] G. Kowarik, R. J. Bereczky, F. Aumayr, and K. Tökési, Nucl. Instrum. Methods Phys. Res. Sect. B **267**, 2277 (2009).
[13] R. Nakayama, M. Tona, N. Nakamura, H. Watanabe, N. Yoshiyasu, C. Yamada, A. Yamazaki, S. Ohtani, and M. Sakurai, Nucl. Instrum. Methods Phys. Res. Sect. B **267**, 2381 (2009).
[14] E. Gruber, G. Kowarik, F. Ladening, J. P. Waclawek, F. Aumayr, R. J. Bereczky, K. Tökési, P. Gunacker, T. Schweigler, C. Lemell *et al.*, Phys. Rev. A **86**, 062901 (2012).
[15] T. Ikeda, Y. Kanai, T. M. Kojima, Y. Iwai, T. Kambara, Y. Yamazaki, M. Hoshino, T. Nebiki, and T. Narusawa, Appl. Phys. Lett. **89**, 163502 (2006).
[16] A. Cassimi, T. Muranaka, L. Maunoury, H. Lebius, B. Manil, B. A. Huber, T. Ikeda, Y. Kanai, T. M. Kojima, Y. Iwai *et al.*, Int. J. Nanotechnol. **5**, 809 (2008).
[17] M. Kreller, G. Zschornak, and U. Kentsch, Nucl. Instrum. Methods Phys. Res. Sect. B **269**, 1032 (2011).
[18] G. P. Pokhil and V. V. Cherdyntsev, J. Surf. Investig. **7**, 356 (2013).
[19] F. Aumayr, S. Facsko, A. S. El-Said, C. Trautmann, and M. Schleberger, J. Phys.: Condens. Matter **23**, 393001 (2011).
[20] H. Q. Zhang, N. Akram, P. Skog, I. Soroka, C. Trautmann, and R. Schuch, Phys. Rev. Lett. **108**, 193202 (2012).
[21] D. Tomono, T. Kojima, K. Ishida, T. Ikeda, Y. Iwai, M. Tokuda, Y. Kanazawa, Y. Matsuda, T. Matsuzaki, M. Iwasaki *et al.*, J. Phys. Soc. Jpn. **80**, 044501 (2011).
[22] Y. Iwai, T. Ikeda, T. Kojima, Y. Yamazaki, K. Maeshima, N. Imamoto, T. Kobayashi, T. Nebiki, T. Narusawa, and G. P. Pokhil, Appl. Phys. Lett. **92**, 023509 (2008).
[23] K. Schiessl, W. Palfinger, C. Lemell, and J. Burgdörfer, Nucl. Instrum. Methods Phys. Res. Sect. B **232**, 228 (2005).
[24] K. Schiessl, W. Palfinger, K. Tökési, H. Nowotny, C. Lemell, and J. Burgdörfer, Phys. Rev. A **72**, 062902 (2005).
[25] K. Schiessl, W. Palfinger, K. Tökési, H. Nowotny, C. Lemell, and J. Burgdörfer, Nucl. Instrum. Methods Phys. Res. Sect. B **258**, 150 (2007).
[26] T. Schweigler, C. Lemell, and J. Burgdorfer, Nucl. Instrum. Methods Phys. Res. Sect. B **269**, 1253 (2011).
[27] N. Stolterfoht, Phys. Rev. A **87**, 012902 (2013).
[28] N. Stolterfoht, Phys. Rev. A **87**, 032901 (2013).
[29] J. Frenkel, Phys. Rev. **54**, 647 (1938).
[30] N. Stolterfoht, Phys. Rev. A **89**, 062706 (2014).
[31] N. Stolterfoht, Nucl. Instrum. Methods Phys. Res. Sect. B (to be published).
[32] Borosilicate glass (Duran) from www.duran-group.com.
[33] E. Gruber, N. Stolterfoht, P. Allinger, S. Wampla, Y. Wang, M. J. Simon, and F. Aumayr, Nucl. Instrum. Methods Phys. Res. Sect. B **340**, 1 (2014).
[34] D. Manura and D. Dahl, Scientific Instrument Services, Ringoes, NJ 08551, 2008, http://simion.com.
[35] P. Love, J. Phys. C **16**, 5985 (1983).
[36] E. Galutschek, R. Trassl, E. Salzborn, F. Aumayr, and H. Winter, J. Phys. Conf. Proc. **58**, 395 (2007).